



## Magnetoelectric effects of nanoparticulate $\text{Pb}(\text{Zr}_{0.52}\text{Ti}_{0.48})\text{O}_3 - \text{NiFe}_2\text{O}_4$ composite films

Hyejin Ryu, P. Murugavel, J. H. Lee, S. C. Chae, T. W. Noh, Yoon Seok Oh, Hyung Jin Kim, Kee Hoon Kim, Jae Hyuck Jang, Miyoung Kim, C. Bae, and J.-G. Park

Citation: *Applied Physics Letters* **89**, 102907 (2006); doi: 10.1063/1.2338766

View online: <http://dx.doi.org/10.1063/1.2338766>

View Table of Contents: <http://scitation.aip.org/content/aip/journal/apl/89/10?ver=pdfcov>

Published by the AIP Publishing

---

### Articles you may be interested in

Multiferroic and magnetoelectric properties of  $\text{CoFe}_2\text{O}_4/\text{Pb}_{1-x}\text{Sr}_x\text{TiO}_3$  composite films

J. Appl. Phys. **117**, 164101 (2015); 10.1063/1.4918663

Magneto-electric effects in functionally stepped magnetic nanobilayers on ferroelectric substrates: Observation and theory on the influence of interlayer exchange coupling

J. Appl. Phys. **115**, 193909 (2014); 10.1063/1.4878458

Controlled self-assembly of multiferroic core-shell nanoparticles exhibiting strong magneto-electric effects

Appl. Phys. Lett. **104**, 052901 (2014); 10.1063/1.4863690

Magnetoelectric effect of mildly conducting magnetostrictive/piezoelectric particulate composites


J. Appl. Phys. **100**, 043910 (2006); 10.1063/1.2245194

Theory of low-frequency magnetoelectric effects in ferromagnetic-ferroelectric layered composites


J. Appl. Phys. **92**, 7681 (2002); 10.1063/1.1522834

---


Frustrated by old technology?



Is your AFM dead and can't be repaired?



Sick of bad customer support?




**It is time to upgrade your AFM**

Minimum \$20,000 trade-in discount for purchases before August 31st

**Asylum Research is today's technology leader in AFM**

[dropmyoldAFM@oxinst.com](mailto:dropmyoldAFM@oxinst.com)



# Magnetoelectric effects of nanoparticulate $\text{Pb}(\text{Zr}_{0.52}\text{Ti}_{0.48})\text{O}_3\text{--NiFe}_2\text{O}_4$ composite films

Hyejin Ryu, P. Murugavel, J. H. Lee, S. C. Chae, and T. W. Noh<sup>a)</sup>

*ReCOE, and FPRD, School of Physics and Astronomy, Seoul National University, Seoul 151-747, Korea*

Yoon Seok Oh, Hyung Jin Kim, and Kee Hoon Kim

*XMPL, and FPRD, School of Physics and Astronomy, Seoul National University, Seoul 151-747, Korea*

Jae Hyuck Jang and Miyoung Kim

*School of Materials Science and Engineering, Seoul National University, Seoul 151-747, Korea*

C. Bae and J.-G. Park

*Department of Physics, Sungkyunkwan University, Suwon 440-746, Korea*

(Received 3 June 2006; accepted 2 July 2006; published online 8 September 2006)

The authors fabricated  $\text{Pb}(\text{Zr}_{0.52}\text{Ti}_{0.48})\text{O}_3\text{--NiFe}_2\text{O}_4$  composite films consisting of randomly dispersed  $\text{NiFe}_2\text{O}_4$  nanoparticles in the  $\text{Pb}(\text{Zr}_{0.52}\text{Ti}_{0.48})\text{O}_3$  matrix. The structural analysis revealed that the crystal axes of the  $\text{NiFe}_2\text{O}_4$  nanoparticles are aligned with those of the ferroelectric matrix. The composite has good ferroelectric and magnetic properties. The authors measured the transverse and longitudinal components of the magnetoelectric voltage coefficient, which supports the postulate that the magnetoelectric effect comes from direct stress coupling between magnetostrictive  $\text{NiFe}_2\text{O}_4$  and piezoelectric  $\text{Pb}(\text{Zr}_{0.52}\text{Ti}_{0.48})\text{O}_3$  grains. © 2006 American Institute of Physics.  
[DOI: 10.1063/1.2338766]

Magnetoelectric (ME) materials have attracted much research interest due to the coupling among the electric, magnetic, and elastic order parameters.<sup>1–4</sup> The figure of merit for ME materials is the magnetoelectric voltage coefficient ( $\alpha_E$ ), which represents the amount of polarization induced under a given applied magnetic field.<sup>5</sup> Many workers have tried to combine perovskite ferroelectrics [such as  $\text{BaTiO}_3$  and  $\text{Pb}(\text{Zr},\text{Ti})\text{O}_3$ ] with spinel ferromagnetic materials (such as  $\text{CoFe}_2\text{O}_4$  and  $\text{NiFe}_2\text{O}_4$ ) to improve the  $\alpha_E$  value in numerous bulk composites.<sup>6–9</sup> Recently, Zheng *et al.* reported a thin film type of ME material, composed of self-assembled  $\text{CoFe}_2\text{O}_4$  spinel nanopillars in a  $\text{BaTiO}_3$  perovskite matrix on a single crystal substrate.<sup>10</sup> In this intriguing composite thin film, nanopillars and matrix materials were grown with a high degree of crystallographic orientation. Good connectivity among the constituents might result in significant coupling between the piezoelectric and magnetostrictive phases to enhance the ME effects. However, no direct evidence of such ME effects has been reported yet.<sup>10,11</sup>

In this letter, we report another type of thin film composite ME material, in which ferromagnetic nanoparticles are dispersed with their crystal orientations aligned in the ferroelectric matrix. Since the ferromagnetic  $\text{NiFe}_2\text{O}_4$  (NFO) phase exists as nanoparticles, instead of nanopillars, its microstructure can reduce possible leakage current paths through the ferromagnetic phase substantially. As a model system, we selected the  $0.65\text{Pb}(\text{Zr}_{0.52}\text{Ti}_{0.48})\text{O}_3$  (PZT)– $0.35\text{NiFe}_2\text{O}_4$  (NFO) system due to its high piezoelectric and magnetostrictive properties.<sup>9</sup>

We fabricated the PZT–NFO films on (001) oriented 0.5% Nb-doped  $\text{SrTiO}_3$  (Nb:STO) substrates using pulsed laser deposition. We used a KrF excimer laser (248 nm, Lambda Physik), with laser fluence and repetition rates of

1 J/cm<sup>2</sup> and 3 Hz, respectively. We deposited the films at 600 °C at an oxygen partial pressure of 100 mTorr. To obtain the 0.65PZT–0.35NFO composite films, we used a modified target, joined by two sintered semicircular disks of PZT and NFO. We carefully chose the disk sizes and target rotations and confirmed the composition of our deposited PZT–NFO films using electron probe microscope analysis.

The constituents of the PZT–NFO composite film have their crystal orientations aligned with respect to the substrate. Figure 1(a) shows the x-ray diffraction (XRD)  $\theta$ - $2\theta$  pattern around the (002) Nb:STO peak, measured using the synchrotron radiation source at Pohang Light Source, Korea. The distinct set of PZT and NFO peaks confirms that the film contained coexisting PZT and NFO phases with no impurity phases. In addition, the perovskite PZT (002) and spinel NFO (004) peaks indicate that their *c* axes should be aligned perpendicular to the substrate. Figure 1(b) displays the  $\phi$  scan data recorded around the NFO (404), PZT (202), and Nb:STO (202) reflections, which show a set of four distinct peaks with 90° of separation. These XRD data confirm that the NFO and PZT grains are aligned in a specific orientation, such as (001) NFO|| (001) PZT|| (001) Nb:STO and [100] NFO|| [100] PZT|| [100] Nb:STO.

To obtain further microstructural information, we performed transmission electron microscope (TEM) studies with a Tecnai 20F field emission microscope. Figure 2(a) shows a low-resolution TEM image, in which the marked regions indicate that the NFO nanoparticles are well dispersed in the PZT matrix. We also obtained high-resolution images near the NFO–PZT boundary, as shown in Figs. 2(b) and 2(c). Figure 2(c) shows a well-defined boundary with clear atomic arrangements of the PZT matrix and NFO nanoparticles. We could index the spots in the selected-area electron diffraction patterns, shown in Fig. 2(d), to PZT (220) and NFO (440). Both Figs. 2(c) and 2(d) indicate that the particles in the composite film are aligned with the [100]

<sup>a)</sup> Author to whom correspondence should be addressed; electronic mail: twnoh@snu.ac.kr

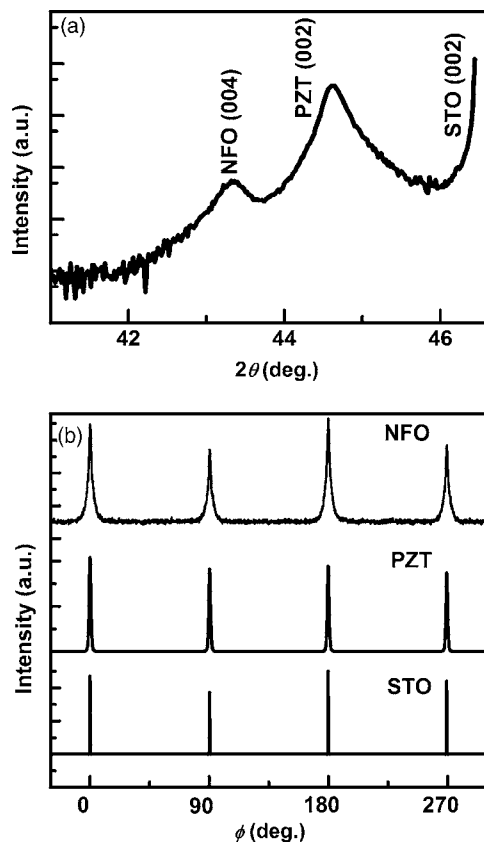


FIG. 1. (a)  $\theta$ - $2\theta$  XRD scan of a PZT-NFO composite film on Nb:STO substrate. (b)  $\phi$  scans recorded on NFO (404), PZT (202), and Nb:STO (202) reflections.

NFO[100] PZT relationship. These TEM studies confirm that the NFO nanoparticles are dispersed randomly in the PZT matrix, as shown schematically in Fig. 2(e). This microstructure differs from that of the self-assembled nanopillars,<sup>10</sup> shown schematically in Fig. 2(f). The microstructure of our PZT-NFO composite film could significantly reduce leakage current paths in the ferroelectric and ME measurements.

Our PZT-NFO composite film demonstrated good ferroelectric and ferromagnetic properties. We measured the polarization versus electric field ( $P$ - $E$ ) curves at various applied electric fields using a precision workstation (Radiant Technologies). As shown in Fig. 3(a), the measured  $P$ - $E$  loops had good ferroelectric characteristics: the remnant polarization, saturation polarization, and coercive field at the applied electric field of 800 kV/cm were 45  $\mu\text{C}/\text{cm}^2$ , 60  $\mu\text{C}/\text{cm}^2$ , and 275 kV/cm, respectively. These values are comparable to those of reported PZT films,<sup>12</sup> which indicate that the PZT phase retains its good quality in the composite film. We also performed magnetization versus field ( $M$ - $H$ ) measurements using a Quantum Design magnetic property measurement system. Figure 3(b) shows the measured  $M$ - $H$  loop with the magnetic field applied in the direction of the plane. The values of saturation magnetization and coercive field turned out to be about 35  $\text{emu}/\text{cm}^3$  and 70 Oe, respectively. When we scale saturation magnetization value by the volume fraction of NFO, the normalized value (i.e., 100  $\text{emu}/\text{cm}^3$ ) is in good agreement with the reported value for the NFO films (i.e., about 135  $\text{emu}/\text{cm}^3$ ).<sup>13</sup>

To determine the  $\alpha_E$  values of our PZT-NFO composite film, we performed ME susceptibility measurements using a

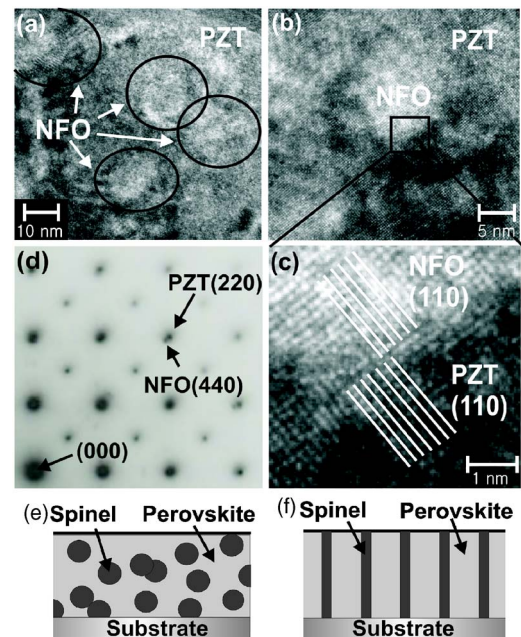


FIG. 2. (a) Low-magnification high-resolution transmission electron microscopy (HRTEM) image of the PZT-NFO film. The marked regions indicate the NFO phase. (b) HRTEM image near the PZT-NFO boundary and (c) an enlarged image of the region marked in (b). (d) Selected-area electron diffraction pattern of the composite film. Schematic representations of a composite film with spinel phase growth involving (e) nanoparticles and (f) self-assembled nanopillars.

homemade setup. After poling, the  $\alpha_E$  values are deduced from the charge ( $\delta Q$ ) generated from the sample by applying an ac magnetic field ( $\delta H$ ) at a frequency of 194 Hz, under the dc magnetic bias ( $H_B$ ):  $\alpha_E = \delta Q / (\delta H d C)$ , where  $d$  and  $C$  are the thickness and capacitance of the film, respectively. Details of the measurement scheme will be published

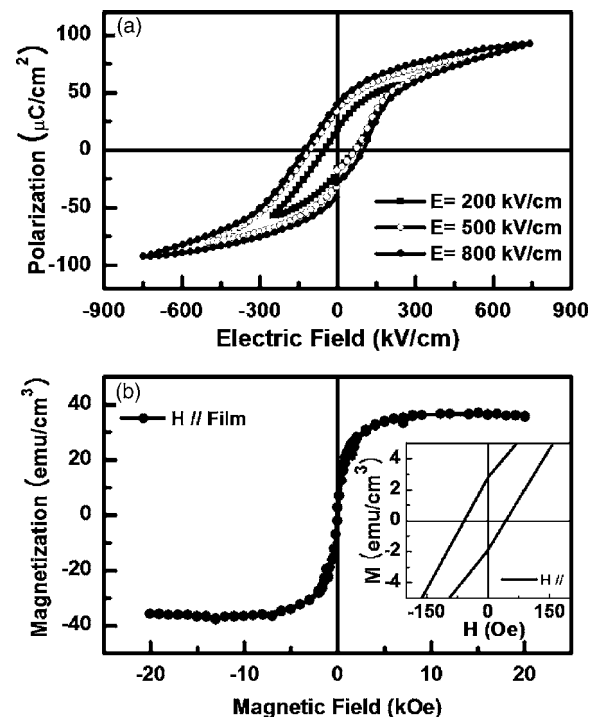


FIG. 3. (a) Polarization hysteresis loops of the composite film measured at various electric fields. (b) Magnetization curve with respect to the magnetic field in the field in-plane direction of the sample.



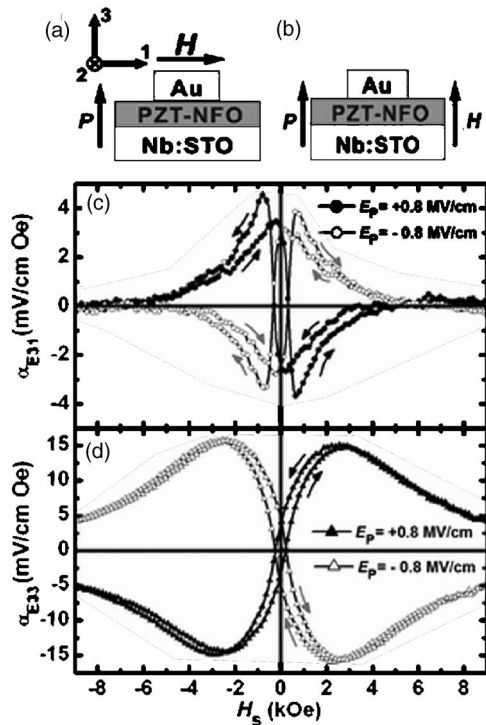


FIG. 4. Schematic diagrams showing the experimental configuration for the (a) transverse ( $\alpha_{E31}$ ) and (b) longitudinal ( $\alpha_{E33}$ ) components of the magnetoelectric coefficient. (c)  $\alpha_{E31}$  and (d)  $\alpha_{E33}$  measured on the composite film after poling at +0.8 and -0.8 MV/cm.

elsewhere.<sup>14</sup> Figure 4(a) shows the experimental configuration of the transverse components of  $\alpha_E$  ( $\alpha_{E31}$ ) schematically when we measured  $\delta Q_{||}[001]$  (i.e., along axis 3) while applying both  $H_B$  and  $dH$  along  $[100]$  (i.e., along axis 1). Figure 4(b) shows a similar schematic diagram for the longitudinal components of  $\alpha_E$  ( $\alpha_{E33}$ ) when we applied both the dc and ac magnetic fields along the  $[001]$  direction.

Figures 4(c) and 4(d) show the magnetic field dependent  $\alpha_{E31}$  and  $\alpha_{E33}$ , respectively. The closed and open symbols indicate the results after poling at +0.8 and -0.8 MV/cm, respectively. We measured  $\alpha_{E31}$  and  $\alpha_{E33}$  at various poling electric fields, which indicated saturation behaviors at around 0.8 MV/cm. The maximum value of  $\alpha_{E31}$  was  $\sim 4$  mV/cm Oe, while the corresponding value of  $\alpha_{E33}$  was  $\sim 16$  mV/cm Oe. These values are somewhat lower than the reported  $\alpha_E$  value ( $\sim 37$  mV/cm Oe) of bulk PZT-NFO particulate composites.<sup>7</sup> The smaller values might be due to the lattice clamping effects by the substrate. Figure 4 also shows sign reversal of both  $\alpha_{E31}$  and  $\alpha_{E33}$  between the two oppositely poled states. This demonstrated that the ME signals originated from ferroelectric domains with an inversion symmetry breaking relationship.

One of the important issues concerning composite films is the origin of the ME effects. In our film, both  $\alpha_{E31}$  and  $\alpha_{E33}$  showed sign differences, and the magnitude of  $\alpha_{E33}$  was four times that of  $\alpha_{E31}$ . It has been reported that a single NFO crystal has a positive  $[001]$  magnetostriction ( $\Delta l/l$ ) per-

pendicular to  $H$ , but a negative value parallel to  $H$ .<sup>15</sup> Furthermore, the differential change in the magnetostriction with  $H_{||}[001]$ , i.e.,  $\delta(\Delta l/l)/\delta H$ , is four times larger than that with  $H_{\perp}[001]$ . Therefore, in our composite film geometry, the magnetostriction of the NFO grains along axis 3 causes the lateral length of the PZT matrix to be elongated (shortened) when  $H$  is pointing perpendicular (parallel) to  $[001]$ , resulting in the negative  $\alpha_{E31}$  (positive  $\alpha_{E33}$ ) under a finite  $H_B$  ( $>0$ ). Both the observed sign and magnitude changes in the  $\alpha_E$  coefficients of our composite film imply that its ME effect should come from the magnetostriction coupled lattice constant change of PZT, namely,  $\alpha_E \propto \delta P \propto \delta(\Delta l/l)$ . (In the case of randomly oriented NFO nanoparticles, one would have expected no changes in sign and magnitude of  $\alpha_E$  coefficients.)

In conclusion, we fabricated nanoparticulate  $0.65\text{Pb}(\text{Zr}_{0.52}\text{Ti}_{0.48})\text{O}_3-0.35\text{NiFe}_2\text{O}_4$  composite films, which are composed of randomly dispersed  $\text{NiFe}_2\text{O}_4$  nanoparticles in the  $\text{Pb}(\text{Zr}_{0.52}\text{Ti}_{0.48})\text{O}_3$  matrix. The measured magnetoelectric voltage coefficients of the composite films were comparable to those of bulk particulate composites. Our results also demonstrate that the magnetoelectric effects come from direct stress coupling between the ferroelectric and ferromagnetic grains.

This work was supported by the Creative Research Initiatives (Functionally Integrated Oxide Heterostructures) of MOST/KOSEF. The experiments at Pohang Light Source were supported by MOST and POSTECH. One of the authors (K.H.K.) was supported by the Korean Research Foundation (MOEHRD) (R08-2004-000-10228-0).

<sup>1</sup>T. Kimura, T. Goto, H. Shintani, K. Ishizaka, T. Arima, and Y. Tokura, *Nature (London)* **426**, 55 (2003).

<sup>2</sup>N. Hur, S. Park, P. A. Sharma, J. S. Ahn, S. Guha, and S. W. Cheong, *Nature (London)* **429**, 392 (2004).

<sup>3</sup>N. A. Spaldin and M. Fiebig, *Science* **309**, 391 (2005).

<sup>4</sup>M. W. Kim, S. J. Moon, J. H. Jung, J. Yu, S. Parashar, P. Murugavel, J. H. Lee, and T. W. Noh, *Phys. Rev. Lett.* **96**, 247205 (2006).

<sup>5</sup>M. I. Bichurin, V. M. Petrov, and G. Srinivasan, *Phys. Rev. B* **68**, 054402 (2003).

<sup>6</sup>J. Ryu, S. Priya, K. Uchino, and H. E. Kim, *J. Electroceram.* **8**, 107 (2002).

<sup>7</sup>J. Zhai, N. Cai, Z. Shi, Y. Lin, and C.-W. Nan, *J. Phys. D* **37**, 823 (2004).

<sup>8</sup>J. Zhai, N. Cai, Z. Shi, Y. Lin, and C.-W. Nan, *J. Appl. Phys.* **95**, 5685 (2004).

<sup>9</sup>G. Srinivasan, E. T. Rasmussen, J. Gallegos, R. Srinivasan, Y. I. Bokhan, and V. M. Laletin, *Phys. Rev. B* **64**, 214408 (2001).

<sup>10</sup>H. Zheng, J. Wang, S. E. Lofland, Z. Ma, L. Mohaddes-Ardabili, T. Zhao, L. Salamanca-Riba, S. R. Shinde, S. B. Ogale, F. Bai, D. Viehland, Y. Jia, D. G. Schlom, M. Wuttig, A. Roytburd, and R. Ramesh, *Science* **303**, 661 (2004).

<sup>11</sup>F. Zavaliche, H. Zheng, L. M. Ardabili, S. Y. Yang, Q. Zhan, P. Shafer, E. Reilly, R. Chopdekar, Y. Jia, P. Wright, D. G. Schlom, Y. Suzuki, and R. Ramesh, *Nano Lett.* **5**, 1793 (2005).

<sup>12</sup>I. Kanno, H. Kotera, K. Wasa, T. Matsunaga, T. Kamada, and R. Takayama, *J. Appl. Phys.* **92**, 4091 (2003).

<sup>13</sup>P. Samarasekara and F. J. Cadieu, *Jpn. J. Appl. Phys., Part 1* **40**, 3176 (2001).

<sup>14</sup>Y. S. Oh, H. J. Kim, H. Ryu, T. W. Noh, and K. H. Kim (unpublished).

<sup>15</sup>R. M. Bozorth and J. G. Walker, *Phys. Rev.* **88**, 1209 (1952).